

Supporting Information

Colorimetric and fluorogenic signaling of fluoride ions by diketopyrrolopyrrole-based chemosensor

Xiaofeng Yang, Gege Zhang, Yexin Li, Zheng Liu, Xiaoqian Gong, Bin Gao, Guangyou Zhang, Yu Cui* and Guoxin

Sun*

CONTENTS:

General information

Fig. S1. ^1H NMR spectrum of 3 -----	S3
Fig. S2. ^{13}C NMR spectrum of 3 -----	S3
Fig. S3. ^1H NMR spectrum of 2 -----	S4
Fig. S4. ^{13}C NMR spectrum of 2 -----	S4
Fig. S5. ^1H NMR spectrum of 1 in $\text{DMSO}-d_6$ -----	S5
Fig. S6. ^{13}C NMR spectrum of 1 in $\text{DMSO}-d_6$ -----	S5
Fig. S7. HRMS-ESI spectra of 1 -----	S6
Fig. S8. $^1\text{H}-^1\text{H}$ cosygpsw spectroscopy of 1 in $\text{DMSO}-d_6$ -----	S6
Fig. S9. $^1\text{H}-^{13}\text{C}$ hsqcgp spectroscopy of 1 in $\text{DMSO}-d_6$ -----	S7
Fig. S10. (a) Comparison of partial ^1H NMR spectra of compounds 1 (in CDCl_3) and 2 (in $\text{DMSO}-d_6$). (b) Partial $^1\text{H}-^1\text{H}$ COSY and (c) $^1\text{H}-^{13}\text{C}$ HSQC NMR spectrum of compound 1 (in $\text{DMSO}-d_6$) -----	S8
Fig. S11. Job plot for sensor 1 with fluoride ion-----	S9
Fig. S12. Plot of association constant of sensor 1 with fluoride ion-----	S10
Fig. S13. The limit of detection of sensitivity of sensor 1 for fluoride ion-----	S11
Fig. S14. Time-dependent fluorescence changes of sensor 1 in the presence of F^- -----	S12
Fig. S15. (a) UV-vis absorption and (b) fluorescent spectra of sensor 1 (1×10^{-5} M) to 0-90 equiv. fluoride ions in DMSO. Inset was enlarged spectra as 0-2 equiv. of F^- was added-----	S13
Fig. S16. (a) UV-vis absorption and (b) fluorescent spectra of sensor 1 (1×10^{-5} M) to various amounts of OH^- (as Bu_4N^+ salts)-----	S14
Fig. S17. Partial ^1H NMR titration spectra of sensor 1 (4.7×10^{-3} M) upon addition of increasing amounts of fluoride (TBAF) ion (0-5 equiv.) and F^- alone (top) in $\text{DMSO}-d_6$ -----	S15
Fig. S18. Partial ^{19}F NMR titration spectra of sensor 1 (4.7×10^{-3} M) upon addition of increasing amounts of fluoride (TBAF) ion (0-5 equiv.) and F^- alone (top) in $\text{DMSO}-d_6$ -----	S16
Fig. S19. Quenching curve between sensor 1 and fluoride ion-----	S17
Fig. S20. The emission spectra ($\lambda_{\text{ex}} = 505$ nm) of sensor 1 (1×10^{-5} M) in DMSO in the presence of different concentrations of OH^- followed by the addition of 75 equiv. of fluoride anion in DMSO-----	S18
Fig. S21. UV-vis absorption spectra of 1 (1×10^{-5} M) after addition of 75 equiv. of F^- then 75 equiv. of various anions respectively-----	S18
Fig. S22. Optimized geometries of sensor 1 and 1-2F⁻ complexes at the B3LYP/6-31G* level of theory. The selected bond distances (Å) of the corresponding species are shown-----	S19

Experimental Section

Determination of quantum yield

Fluorescence quantum yield of sensor **1** was determined in DMSO solution by using rhodamine B solution ($\Phi_f = 0.36$, 0.2 μM H₂O) as the reference [1]. The quantum yield was calculated using following equation:

$$\Phi_u = [(A_s F_u n^2) / (A_u F_s n_0^2)] \Phi_s.$$

Where A_s and A_u were the absorbance of the reference and sample solution at the reference excitation wavelength, F_s and F_u were the corresponding integrated fluorescence, n and n_0 were the refractive indexes of the solvents for the sample and reference solutions. Absorbance of samples and references at their respective excitation wavelengths was controlled to be lower than 0.05.

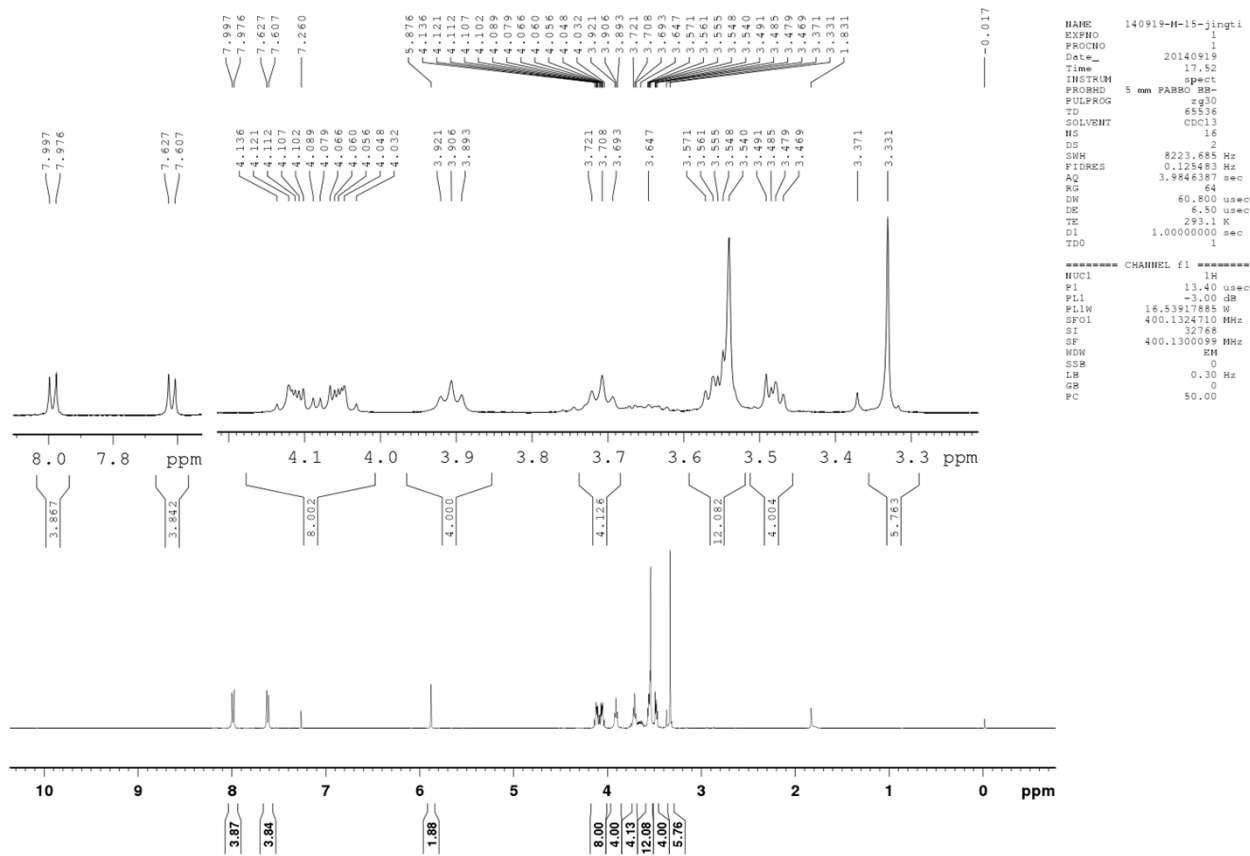
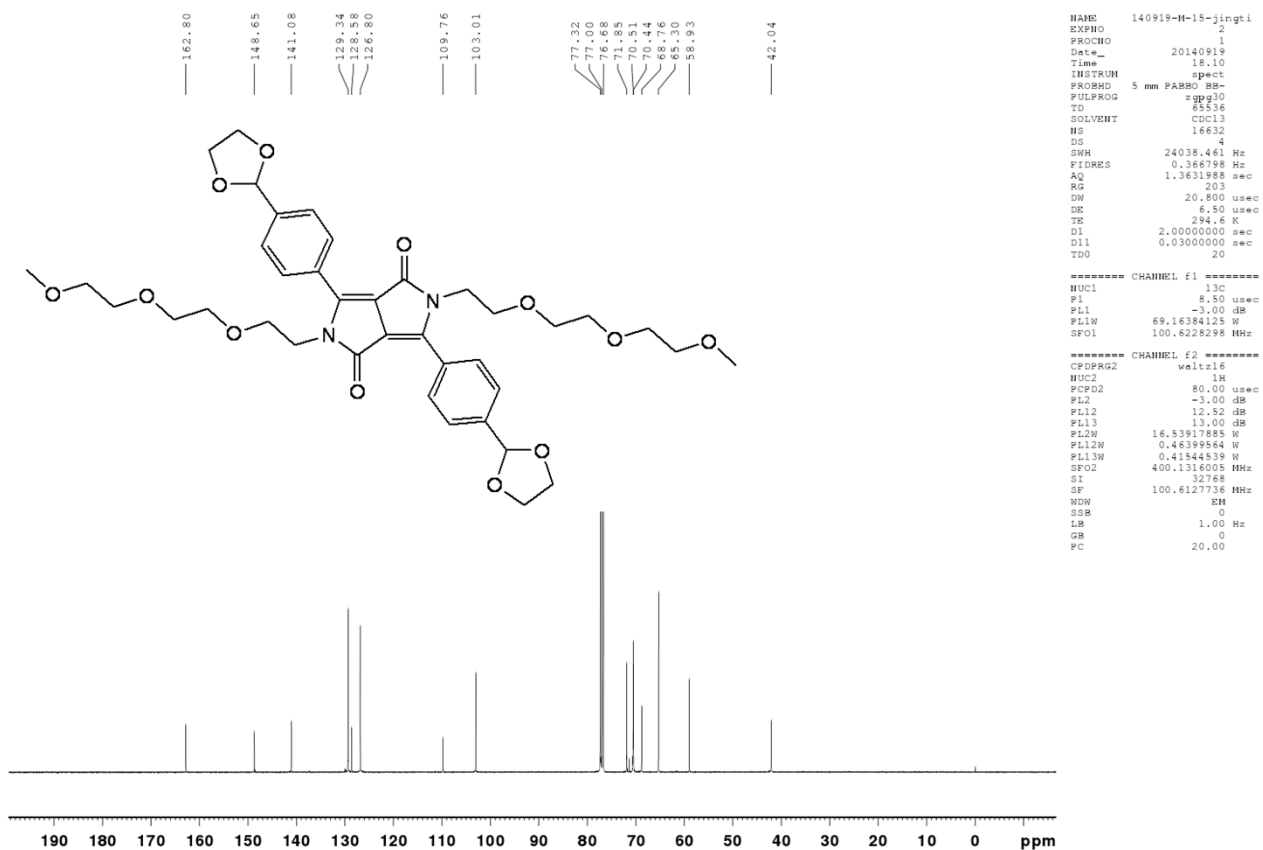


Fig. S1. ¹H NMR spectrum of **3** (CDCl₃, 400 MHz)



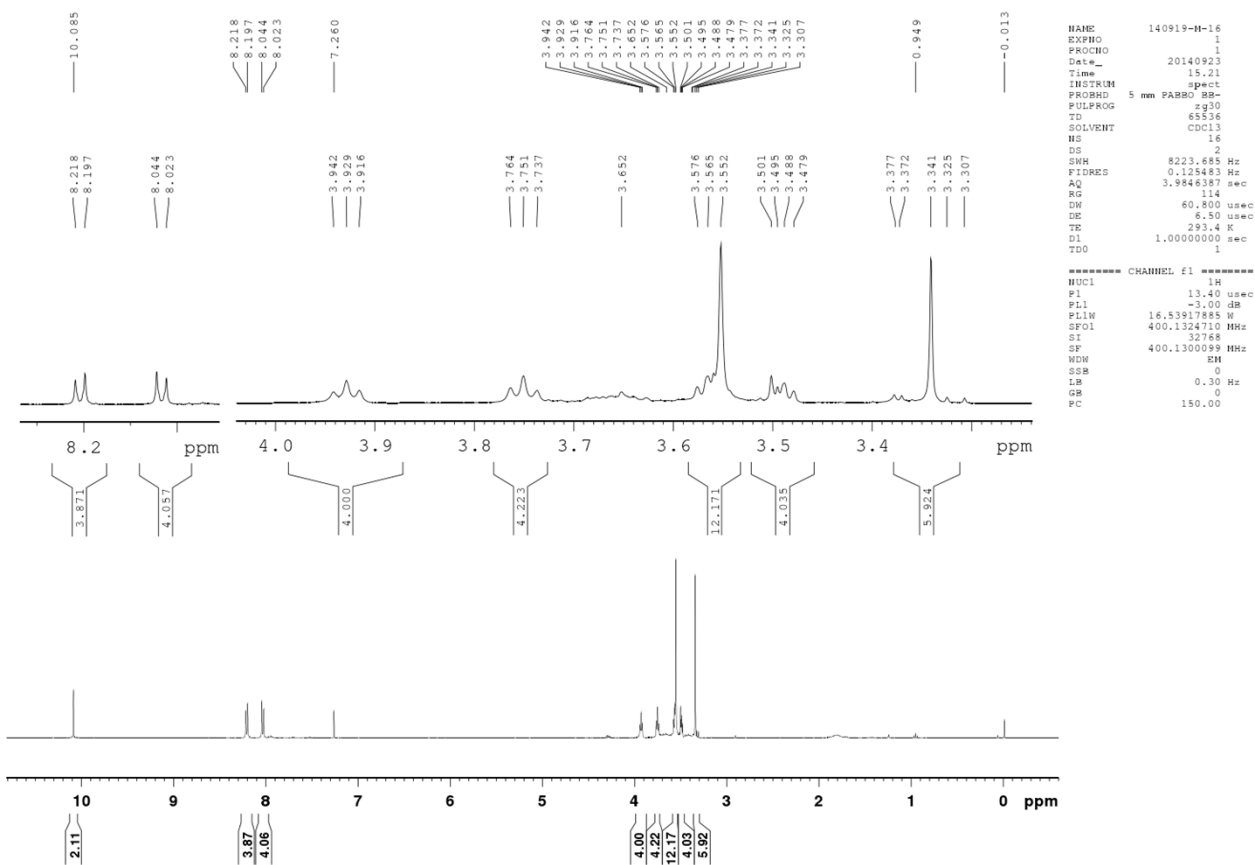


Fig. S3. ¹H NMR spectrum of **2** (CDCl₃, 400 MHz)

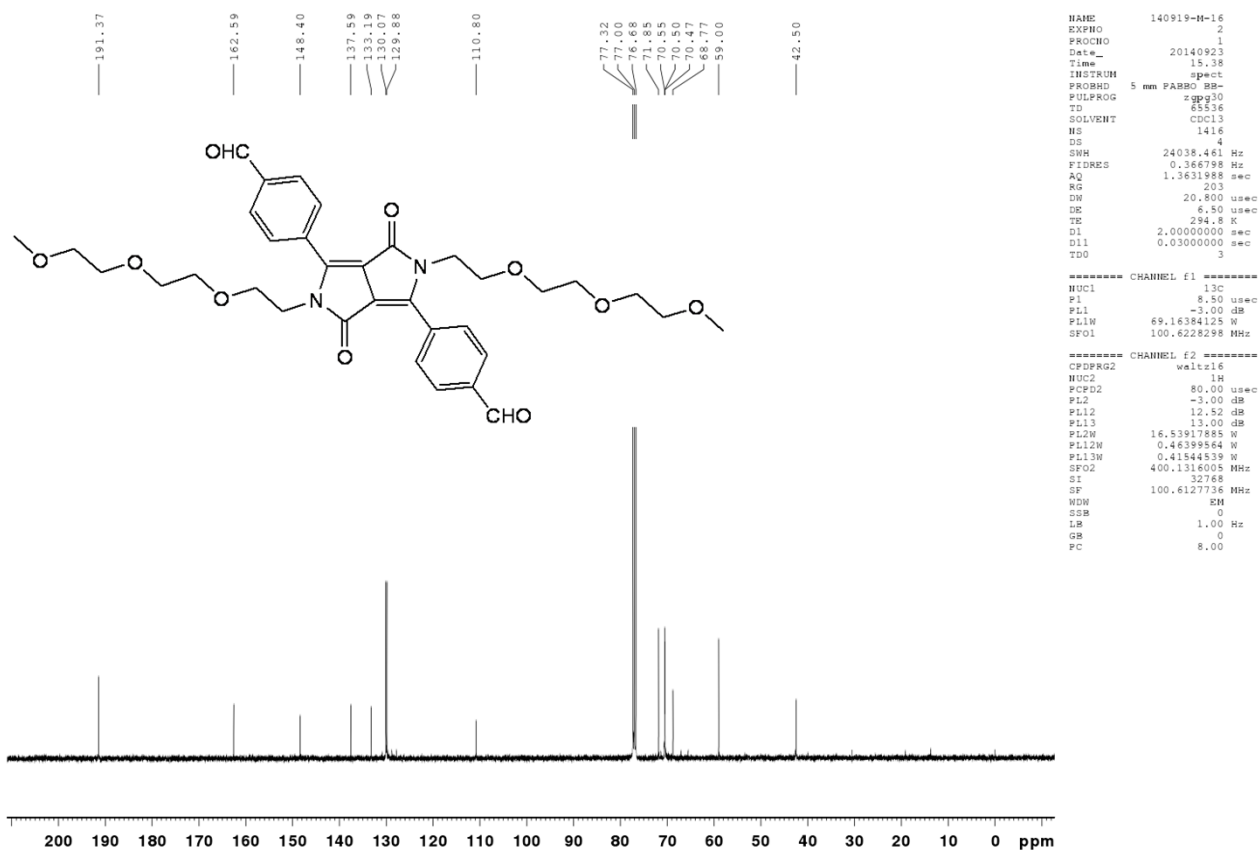


Fig. S4. ¹³C NMR spectrum of **2** (CDCl₃, 100 MHz)

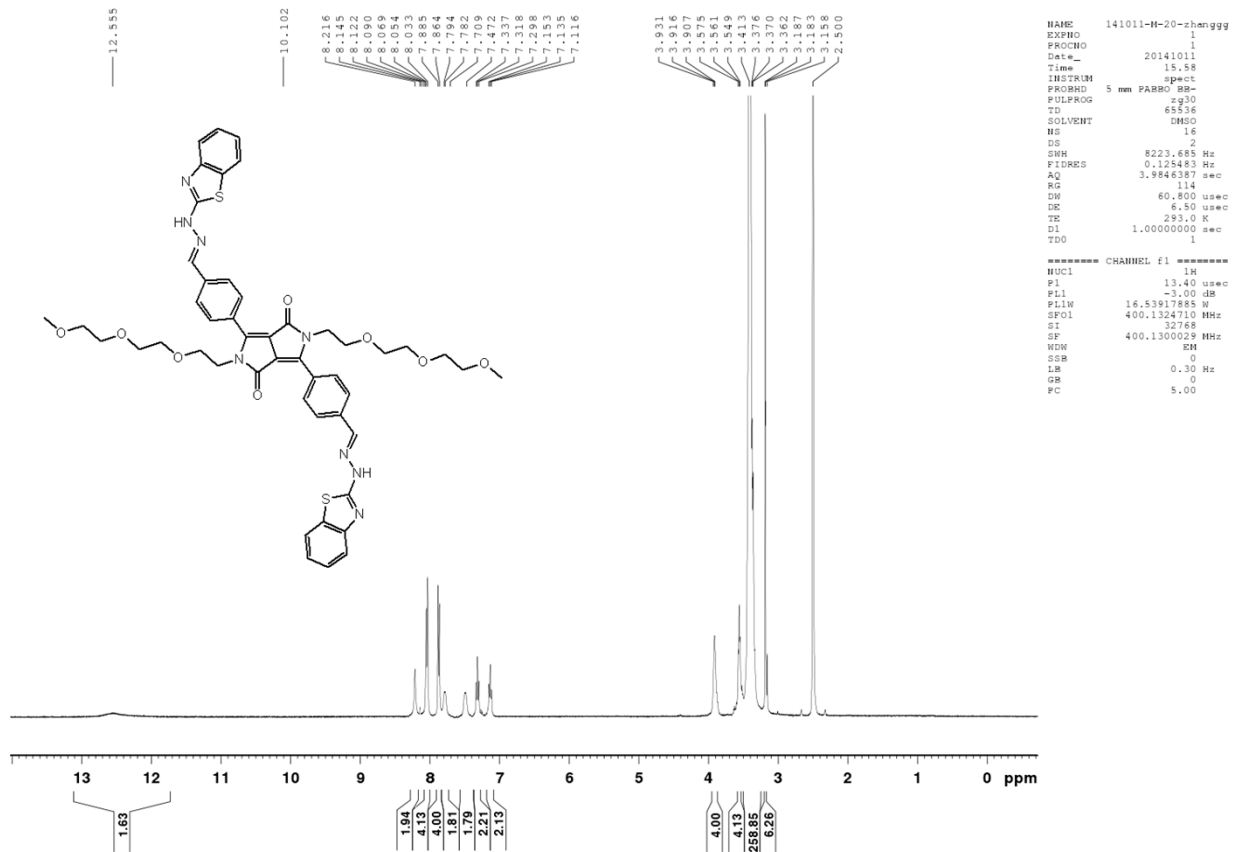


Fig. S5. ¹H NMR spectrum of **1** (DMSO-*d*₆, 400 MHz)

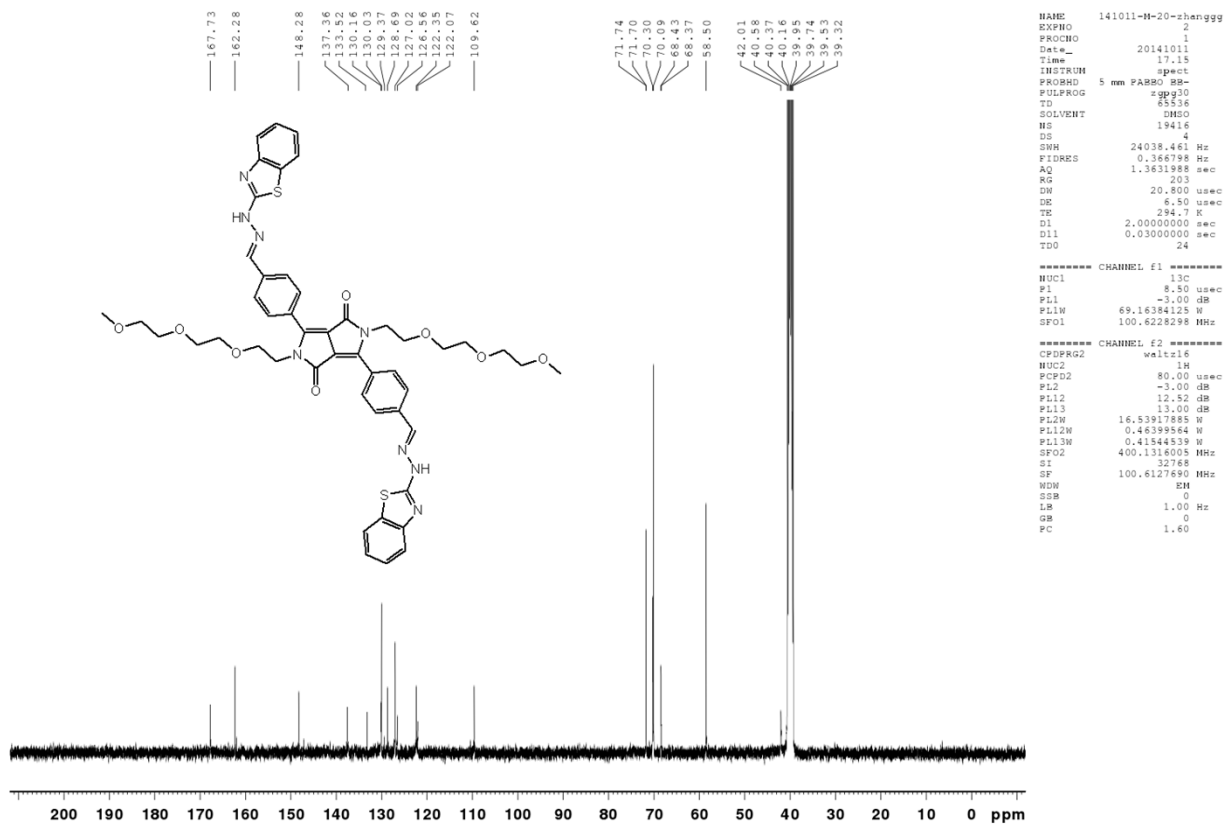


Fig. S6. ¹³C NMR spectrum of **1** (DMSO-*d*₆, 100 MHz)

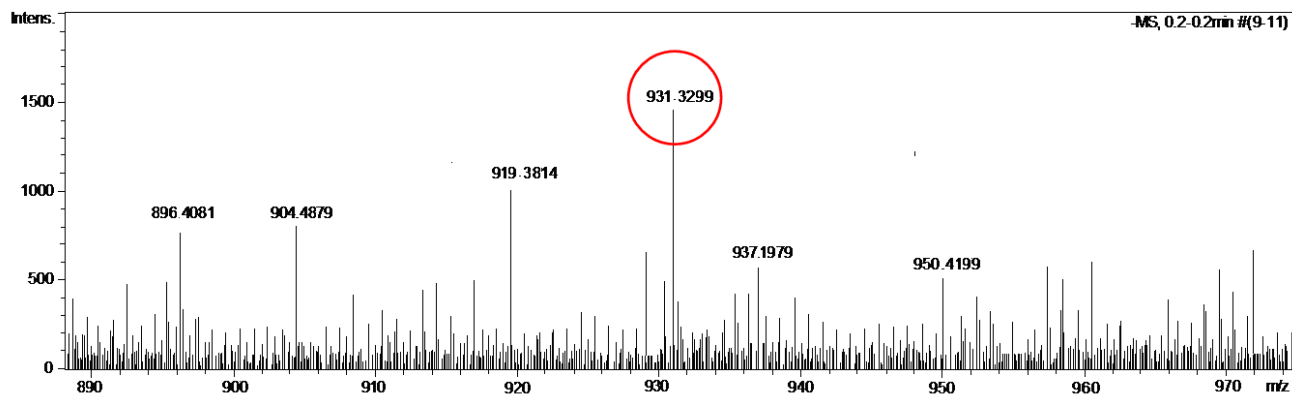


Fig. S7. HRMS-ESI spectra of **1**

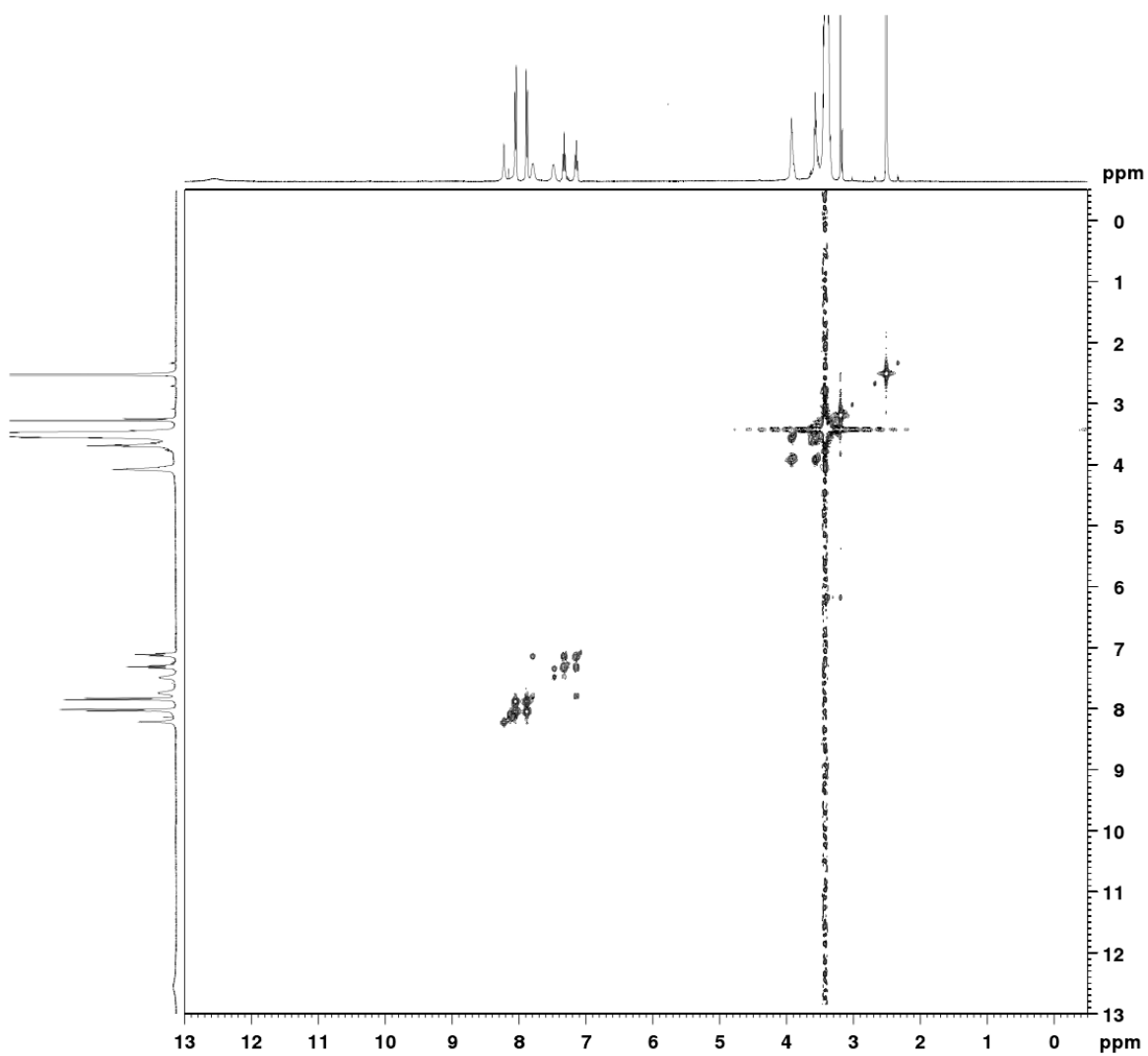


Fig. S8. ^1H - ^1H COSY NMR spectrum of **1** ($\text{DMSO}-d_6$)

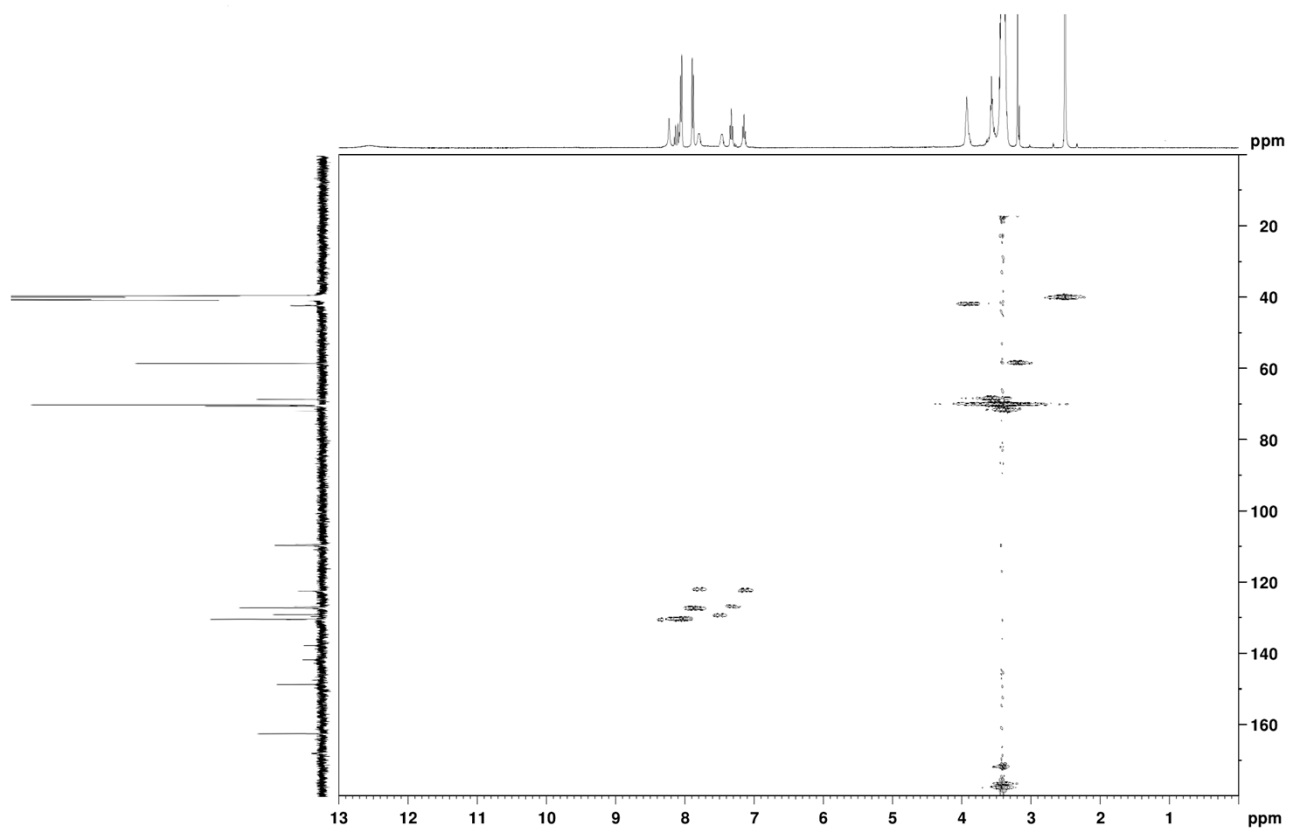


Fig. S9. ^1H - ^{13}C HSQC NMR spectrum of **1** ($\text{DMSO}-d_6$).

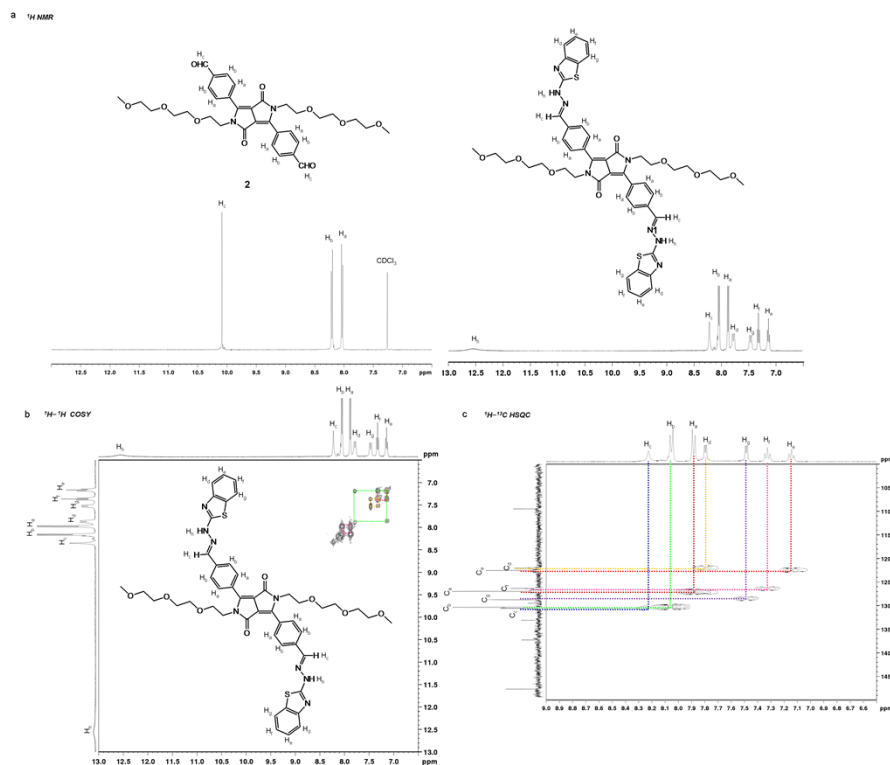


Fig S10. (a) Comparison of partial ¹H NMR spectra of compounds **1** (in CDCl₃) and **2** (in DMSO-*d*₆). (b) Partial ¹H-¹H COSY NMR spectrum of compound **1** (in DMSO-*d*₆). (c) Partial ¹H-¹³C HSQC NMR spectrum of compound **1** (in DMSO-*d*₆).

Fig. S10 showed the comparison of ¹H NMR spectra of compounds **1** (in CDCl₃) and **2** (in DMSO-*d*₆), ¹H-¹H COSY (in DMSO-*d*₆) and ¹H-¹³C HSQC NMR (in DMSO-*d*₆) spectrum of **1**. In ¹H NMR, compound **2** showed a signal at 10.09 ppm which was recognized as the aldehyde proton. However, this signal disappeared and six new signals developed in compound **1** (Fig. S10a). All protons in ¹H NMR spectrum of compound **1** were identified based on the coupling constants, peak integration, and cross-peak correlations observed between the resonances in ¹H-¹H COSY and ¹H-¹³C HSQC spectra (Fig. S10b-c, respectively). In ¹H NMR spectrum of **1**, the doublet resonance at 7.79 ppm which was identified as *H_a*-type aryl proton showed cross-peak correlation with triplet resonance at 7.14 ppm in ¹H-¹H COSY spectrum which was identified as *H_e*-type aryl proton. The triplet resonance at 7.14 ppm which was identified as *H_e*-type aryl proton showed cross-peak correlation with triplet resonance at 7.32 ppm and doublet resonance at 7.79 ppm in COSY spectrum which were identified as *H_f*-type and *H_d*-type aryl protons, respectively. The *H_f*-type resonance at 7.32 ppm showed cross-peak correlation with doublet resonance at 7.46 ppm and triplet resonance at 7.14 ppm in COSY spectrum which were identified as *H_g*-type and *H_e*-type aryl protons, respectively. The doublet resonance at 8.04 ppm which was identified as *H_b*-type *meso*-aryl proton showed cross-peak correlation with doublet resonance at 7.87 ppm in ¹H-¹H COSY spectrum which was identified as *H_a*-type *meso*-aryl proton. The signals at 12.56 ppm and 8.22 ppm (which were identified as *H_h*-type and *H_c*-type protons, respectively) in ¹H NMR spectrum of **1** showed no cross-peak correlation in ¹H-¹H COSY spectrum (Fig. S10b). To assign these two signals of **1**, a ¹H-¹³C HSQC NMR spectrum was measured. As shown in Fig. 1c, the signal at 8.22 ppm in ¹H NMR spectrum of **1** which was identified as *H_c*-type proton showed cross-peak correlation with the signal at 130.2 ppm which was identified as *C_e*-type carbon of hydrazone (CH=N-NH-) in ¹H-¹³C HSQC spectrum. And the signal at 12.56 ppm in ¹H NMR spectrum of **1** which was recognized as *H_h*-type proton showed no cross-peak correlation in ¹H-¹³C HSQC spectra (Fig. S10c). From above analysis, the signal at 12.56 ppm in ¹H NMR spectrum of **1** was recognized as *H_h*-type proton of hydrazone N-H adjacent to C=N bond (CH=N-NH-). Additionally, the aryl protons also identified similarly based on cross-peak correlations in ¹H-¹³C HSQC spectra. The signal at 122.1 ppm which was assigned as *C_d*-type aryl carbon showed cross-peak correlation with a triplet at 7.79 ppm corresponding to *H_a*-type proton. The signal at 122.4 ppm which was assigned as *C_e*-type aryl carbon showed cross-peak correlation with triplet resonance at 7.14 ppm corresponding to *H_e*-type proton. The signal at 126.6 ppm which was assigned as *C_f*-type aryl carbon showed cross-peak correlation with a triplet at 7.32 ppm corresponding to *H_f*-type proton. The signals at 127.0 ppm and 130.0 ppm (which were assigned as *C_a*-type and *C_b*-type aryl carbon, respectively) showed cross-peak correlation with two doublet resonance at 7.87 ppm and 8.04 ppm corresponding to *H_a*-type and *H_b*-type protons, respectively. The signal at 128.7 ppm which was assigned as *C_g*-type aryl carbon showed cross-peak correlation with a doublet resonance at 7.46 ppm corresponding to *H_g*-type proton. Thus, 1D and 2D NMR spectroscopy were very helpful in deducing the molecular structure of compound **1**.

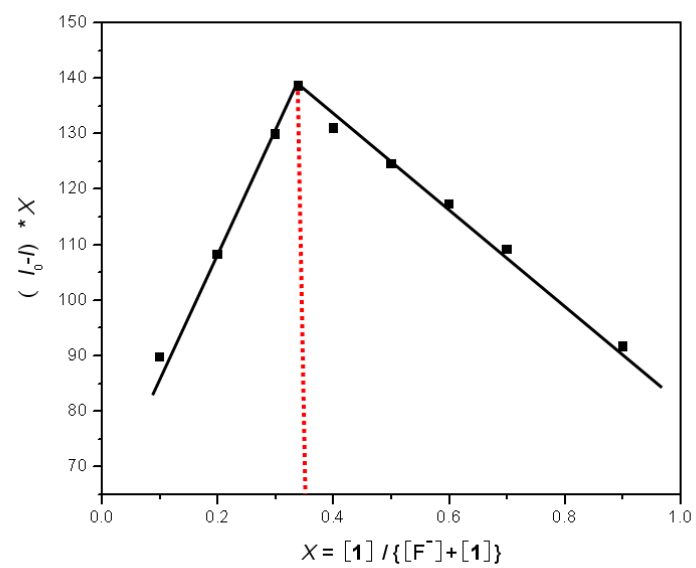


Fig. S11. Job's plot for the evolution of binding stoichiometry between **1** and F^- ion in DMSO solution. The total concentration of $[F^-]$ and **1** was 1.0×10^{-5} M.

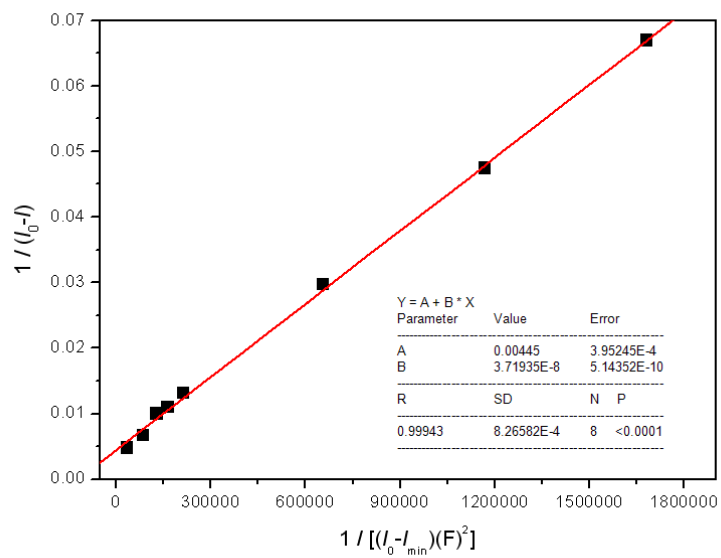


Fig. S12. Benesi-Hildebrand plot of sensor **1** (1.0×10^{-5} M) using 1:2 stoichiometry for association between sensor **1** and fluoride ion. $\lambda_{\text{ex}} = 505$ nm.

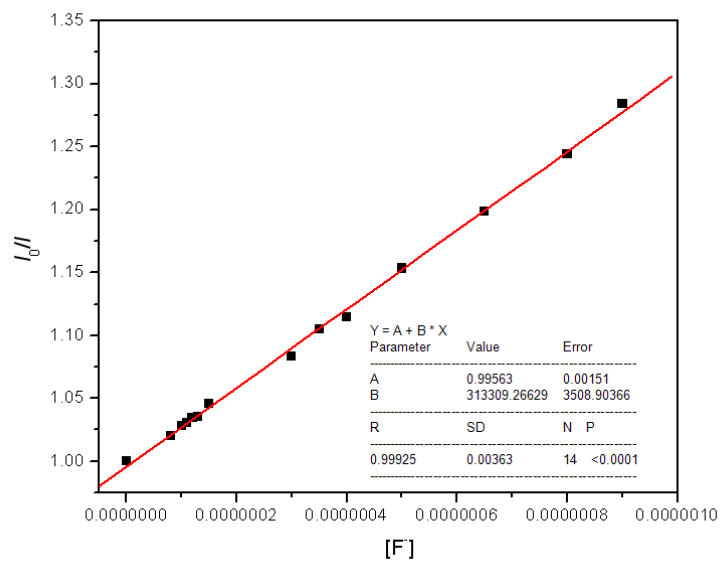


Fig. S13. The linear dynamic fluorescence response for the titration of sensor **1** with F^- to determine the limits of detection (LOD). The LOD was calculated using the formula $3\sigma/k$, where σ = standard deviation of blank (10 samples) and k = the slope of linear calibration curve.

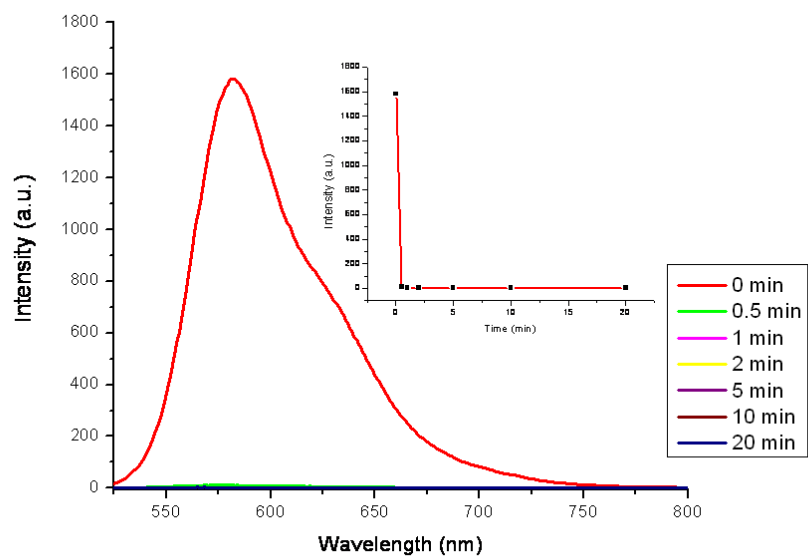


Fig. S14. Time-dependent fluorescence changes of sensor **1** (1×10^{-5} M) in the presence of 75 equiv. of F⁻ in DMSO. $\lambda_{\text{ex}} = 505$ nm.

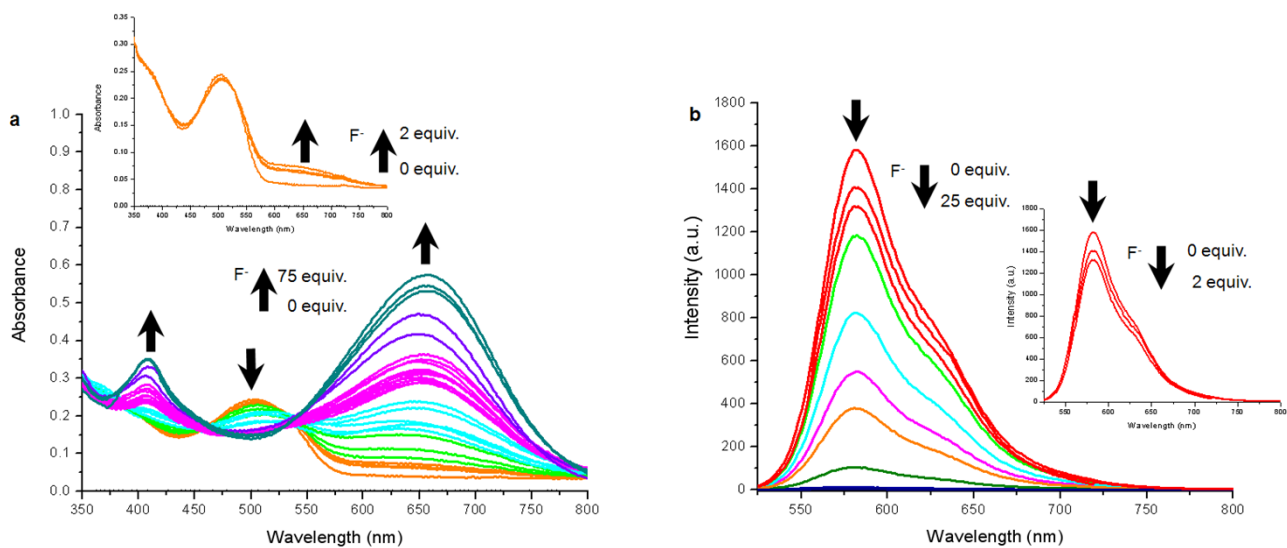


Fig. S15. (a) UV-vis absorption spectra of sensor **1** (1×10^{-5} M) to 0–75 equiv. fluoride ions in DMSO. Inset was enlarged spectra as 0–2 equiv. of F⁻ was added. (b) Fluorescent spectra of sensor **1** (1×10^{-5} M) to 0–25 equiv. fluoride ions in DMSO. Inset was enlarged spectra as 0–2 equiv. of F⁻ was added. λ_{ex} = 505 nm.

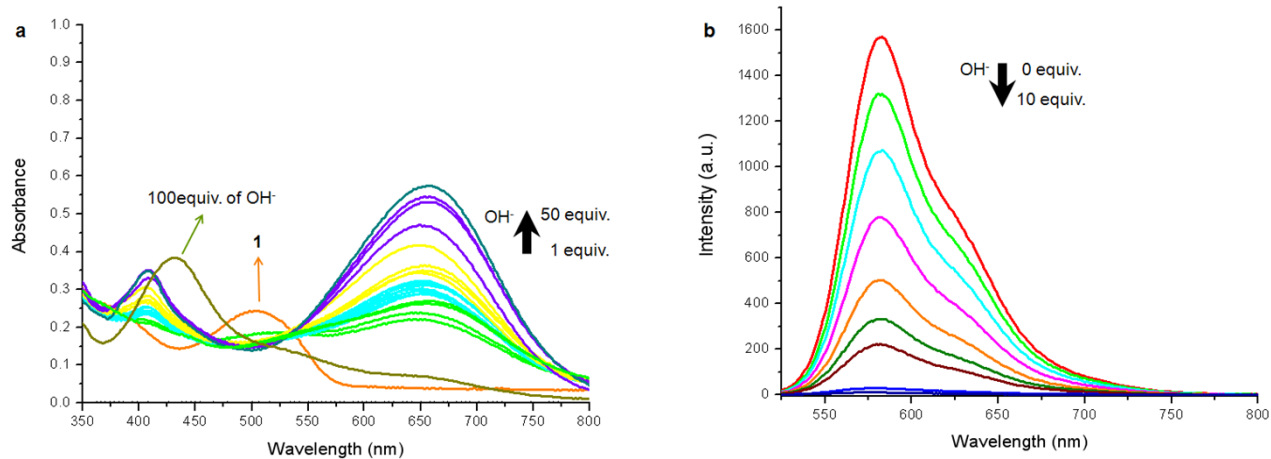


Fig. S16. (a) UV-vis absorption spectra of sensor **1** (1×10^{-5} M) to various amounts of OH^- (as Bu_4N^+ salts). (b) Fluorescent absorption spectra of sensor **1** (1×10^{-5} M) to various amounts of OH^- (as Bu_4N^+ salts). $\lambda_{\text{ex}} = 505$ nm.

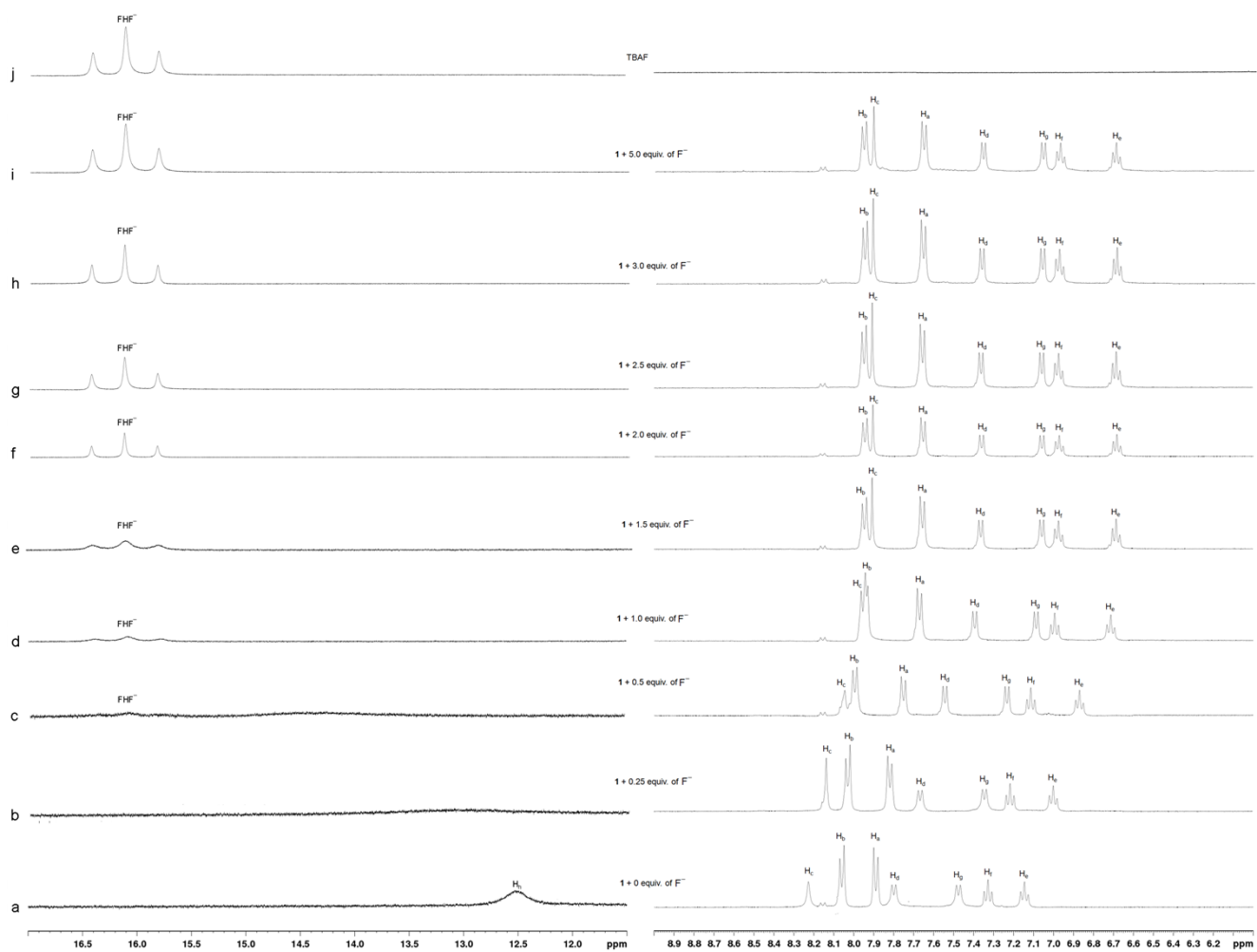


Fig. S17. Partial ^1H NMR titration spectra of sensor **1** (4.7×10^{-3} M) upon addition of increasing amounts of fluoride (TBAF) ion (0–5 equiv.) and F^- alone (top) in $\text{DMSO}-d_6$.

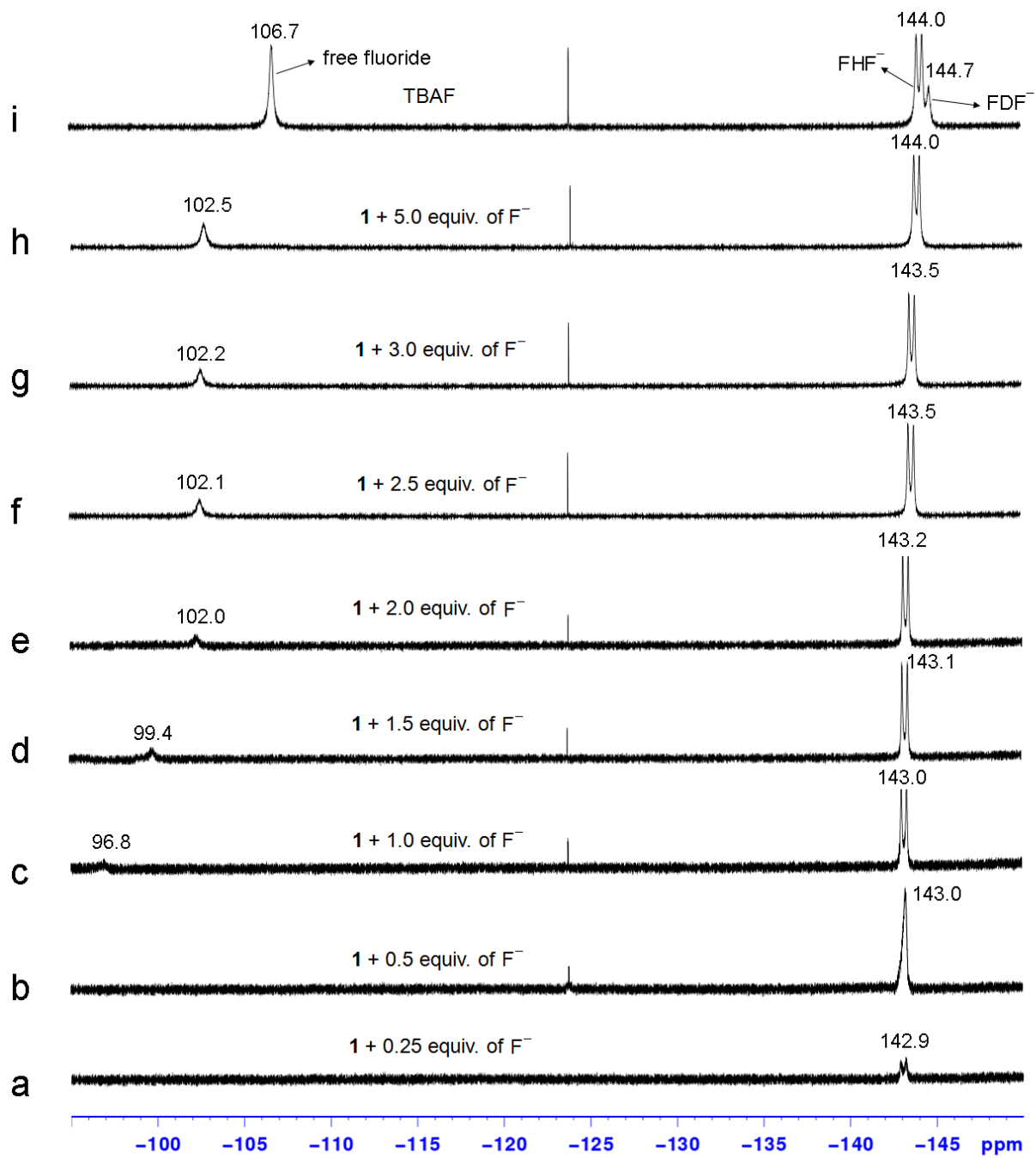


Fig. S18. Partial ^{19}F NMR titration spectra of sensor **1** (4.7×10^{-3} M) upon addition of increasing amounts of fluoride (TBAF) ion (0–5 equiv.) and F^- alone (top) in $\text{DMSO}-d_6$.

The quenching constant was calculated from the spectral titration data by the equation ^[2]:

$$\frac{1}{I_0 - I} = \frac{1}{I_0} + \frac{K_D}{I_0 [F]}$$

Where, I_0 was the fluorescence intensity of sensor, I the fluorescence intensity obtained with fluoride ion, K_D the quenching constant, $[F]$ the concentration of fluoride ion added. Linear fitting of the titration profiles resulted in a good linearity (correlation coefficient was over 0.99) (Fig. S19, Supporting information) and the quenching constant was calculated to be $1.7 \times 10^3 \text{ M}^{-1}$ for **1**.

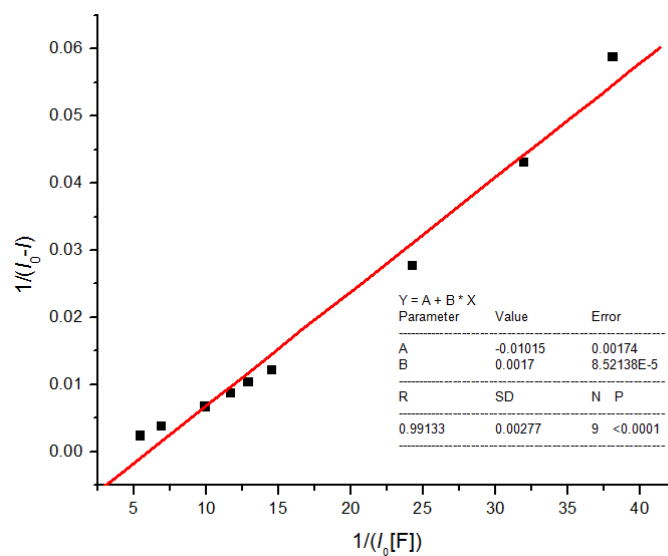


Fig. S19. Quenching curve between sensor **1** and fluoride ion. $\lambda_{\text{ex}} = 505 \text{ nm}$.

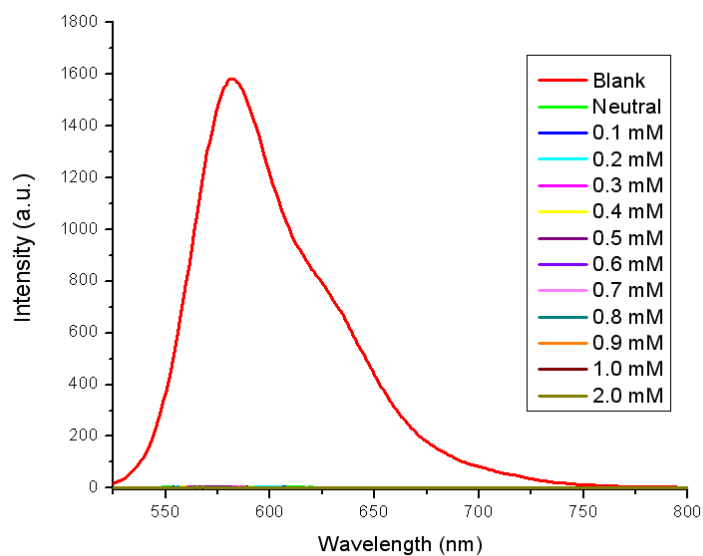


Fig. S20. The emission spectra ($\lambda_{\text{ex}} = 505 \text{ nm}$) of sensor **1** ($1 \times 10^{-5} \text{ M}$) in DMSO in the presence of different concentrations of OH⁻ followed by the addition of 75 equiv. of fluoride anion in DMSO.

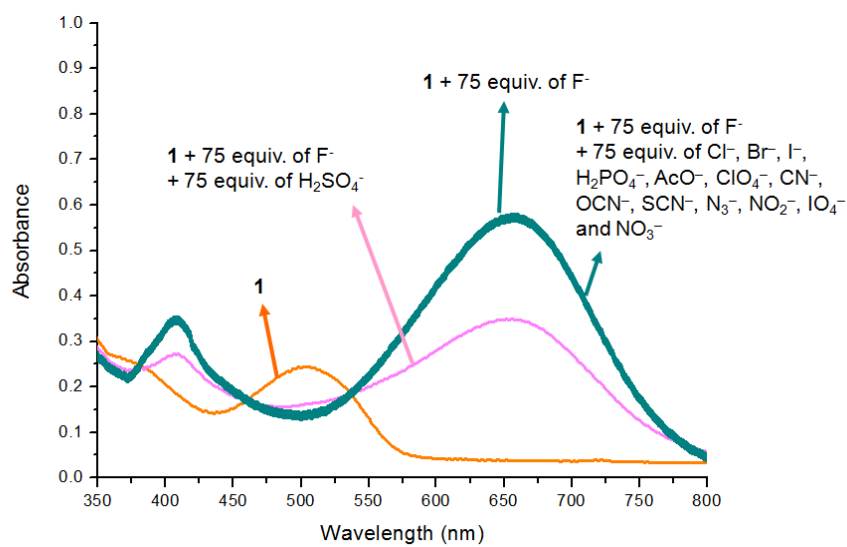


Fig. S21. UV-vis absorption spectra of **1** ($1 \times 10^{-5} \text{ M}$) after addition of 75 equiv. of F⁻ then 75 equiv. of various anions respectively.

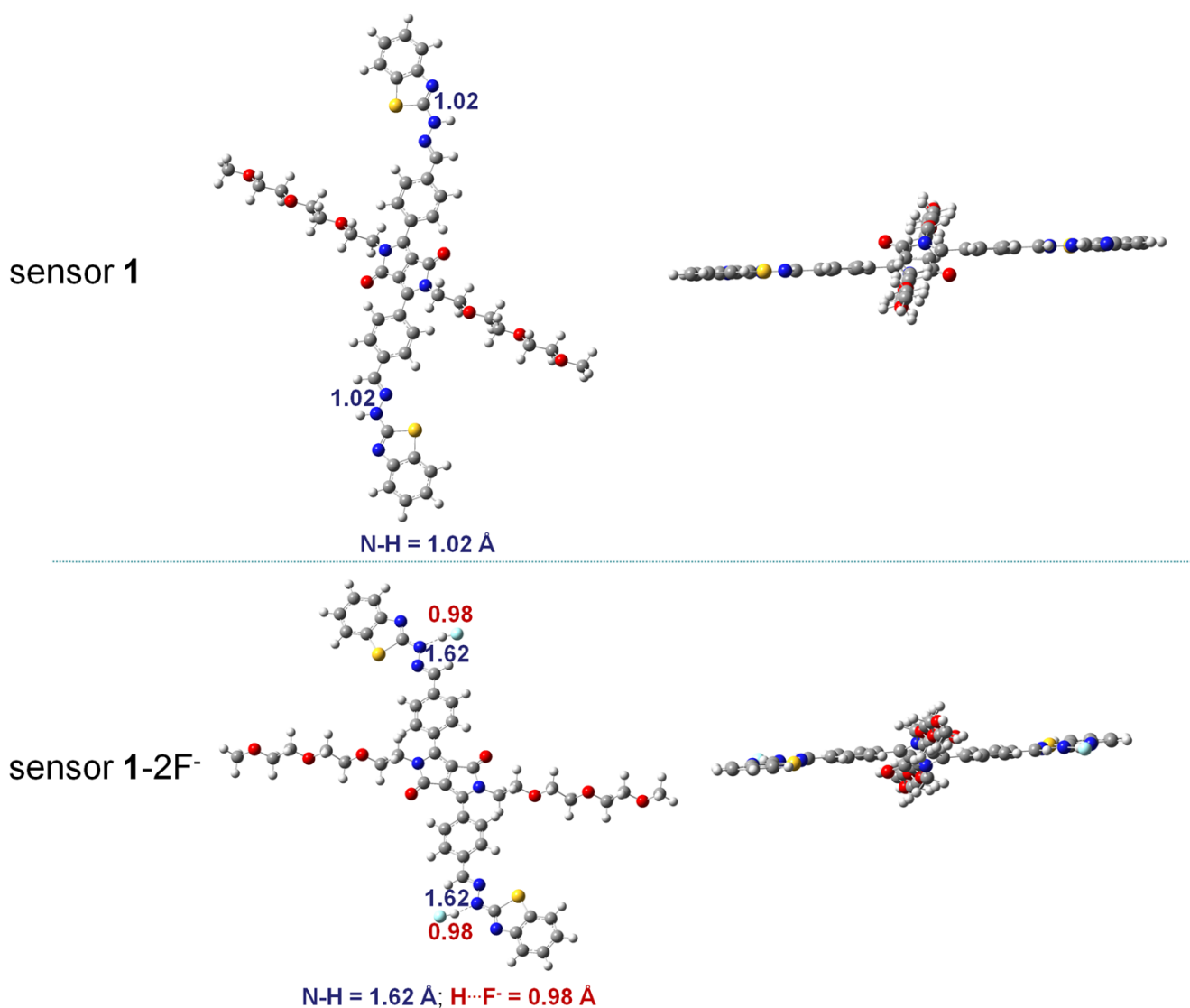


Fig. S22. Optimized geometries of sensor **1** and **1-2F⁻** complexes at the B3LYP/6-31G* level of theory. The selected bond distances (Å) of the corresponding species are shown.

References

- [1] X.-F. Zhang, Y. Zhang, L. Liu, *Journal of Luminescence*, 2014, **145**, 448.
- [2] M. M. Yang, P. Yang, L. W. Zhang, *Chinese Science Bulletin*, 1994, **39**, 31.